Research Article

Sumei Gao*, Longxiang Xu, Chaowu Jin, and Qianwei Chen

Adaptive magnetic suspension anti-rolling device based on frequency modulation

https://doi.org/10.1515/phys-2020-0125
received March 23, 2020; accepted April 4, 2020

Abstract: Joint stabilizers and new technology stabilizers are hotspots of ship stabilizing technology research at the present stage. This study proposes a magnetic suspension stabilizing method; expounds the working principle of magnetic suspension stabilization, respectively; establishes the mathematical model of the magnetic suspension stator and the stabilization mass block and the mathematical model of magnetic stabilizer and ship; and stimulates the displacement, velocity, and acceleration. On the basis of the simulation, a set of magnetic suspension stabilizers have been designed; the stability of suspension has been tested; and, respectively, the acceleration value of stator and stabilization mass block has been measured by loading 0–500 Hz sine voltage excitation signal on electromagnetic coil; thus, the feasibility of the magnetic suspension stabilizer has been verified.

Keywords: magnetic suspension, mathematical model, magnetic stabilizer

1 Introduction

The research on stabilizing devices both at home and abroad mainly concentrated in fin stabilizers [1–3], anti-rolling tank stabilizers [4–6], joint stabilizers, new technology stabilizers, and so on. Joint stabilizers and new technology stabilizers are hotspots of ship stabilizing technology research at the present stage. Kallstrom has demonstrated excellent performance in course control and stabilizing [7]. The stabilizing-anti-overturning integrated balance technique first adopted by INTERING company has been widely used in previous studies [8,9]. Chen and Lai have studied dual-tank stabilizers [10], and Zhao et al. have studied the theory of integrated balance system of large ship [11]. Park et al. suspended stabilization weight via the application of magnetic suspension technology, through the swaying parameters to control the stabilization weight, so as to change the center of gravity of structure and achieve stabilization [12]. Hirakawa et al. have designed a vertical moving stabilization weight on the boat model, by applying the Coriolis effect to achieve stabilization [13]. This study first puts forward another magnetic suspension stabilization technology, describes its working principle, establishes the mathematical model of the magnetic suspension stabilizer to carry out simulation, and then designs the magnetic suspension stabilizer and implements experiments.

2 Constitution and working principle of a magnetic suspension stabilizer

The constitution of a magnetic suspension stabilizer is shown in Figure 1. It consists of the iron core, the electromagnetic coil (stator), the stabilization mass block (rotor), and its control system, of which the stator is fixed on the ship and the rotor (stabilization mass block) is suspended between upper and lower stators in a stable state. Assuming that the ship is suffering from anticlockwise disturbance, anticlockwise rolling, the stabilization mass block will maintain its space position unchanged due to the inertia effect, so the position of the left and right stabilization mass blocks in the stator has changed relatively. The sensors detect the changing

* **Corresponding author: Sumei Gao,** College of Mechanical and Electrical Engineering, Nanjing University of Aeronautics and Astronautics, Nanjing 210016, China; College of Mechanical and Electrical Engineering, Jinling Institute of Technology, Nanjing 211169, China, e-mail: Lxxnuaa@163.com
Longxiang Xu, Chaowu Jin: College of Mechanical and Electrical Engineering, Nanjing University of Aeronautics and Astronautics, Nanjing 210016, China
Qianwei Chen: College of Mechanical and Electrical Engineering, Jinling Institute of Technology, Nanjing 211169, China

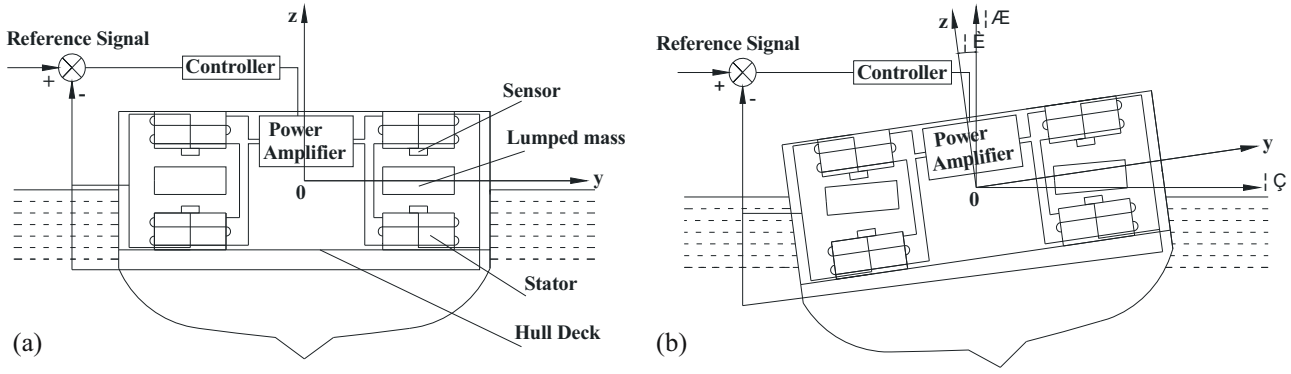

Figure 1: Diagram of stabilizer. (a) Constitution of stabilizer. (b) Working diagram of stabilizer.

positions and send the changing positions to the controller by reference signals; therefore, the current of the stator changed, and then the stabilization mass blocks generate clockwise torque on the stator (hull deck) according to the theory of magnetic levitation. According to the theory of vibration, when the natural frequency of stabilization mass blocks is equal to or approximately the frequency of the disturbance, most of the vibration energy will be concentrated in the stabilization mass blocks, and the hull deck will not vibrate. The ship can be stabilized through the above two functions and *vice versa*.

3 Mathematical model and control

3.1 Mathematical model of the magnetic suspension stator and the stabilization mass block

In Figure 2, upper and lower images are magnetic suspension stators, where M is the quality of the stators, and the stabilization mass block is in the middle, where m is the quality of the block. When the mass block is stably suspended between stators, according to the theory of magnetic suspension stiffness coefficient [14], the displacement stiffness coefficient is calculated as follows:

$$k = -\frac{\mu_0 N^2 A i_{x_0}}{x_0^2}\frac{\mathrm{d}i}{\mathrm{d}x} + \frac{\mu_0 N^2 A i_{x_0}^2}{x_0^3},$$

where μ_0 is the absolute permeability of vacuum, N is the turns of the electromagnet coil, A is the cross-sectional area of the iron core, i_{x_0} is the bias current at the balance position, and x_0 is the gap between the stabilization mass block and the damping mass stator. To overcome anti-rolling mass, the upper bias current should be higher than the lower bias current in order to overcome the weight of the stabilization mass block, namely $i_{x_0} > i_{x_0}$. As the system will adjust the gap between the stator and the stabilization mass block, actual upper and lower bias currents of the system are basically the same, and the upper and lower electromagnet displacement stiffness coefficients are assumed to be k. Assuming that the stator is suffering from upward disturbing force $F_0 \sin \omega t$ and generates upward displacement $x_2(t)$, the displacement is ignored due to less influence of damping on this system, and the equations of motion are obtained as follows:

$$\begin{cases} m\ddot{x}_1(t) = 2k\,[x_2(t) - x_1(t)] \\ M\ddot{x}_2(t) = F_0 \sin \omega t - 2k\,[x_2(t) - x_1(t)] \end{cases} \tag{1}$$

Given

$$\begin{cases} x_1(t) = x_{10} \sin \omega t \\ x_2(t) = x_{20} \sin \omega t \end{cases} \tag{2}$$

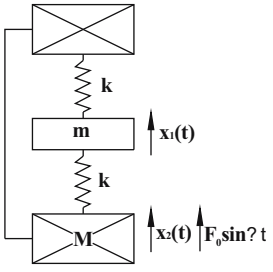

Figure 2: Diagram of the magnetic suspension stator and the stabilization mass block.

Equation (2) is substituted into (1) and we get

$$\begin{cases} x_{10} = \dfrac{2kF_0}{mM\omega^4 - 2k\omega^2(m+M)} \\ x_{20} = \dfrac{(2k - m\omega^2)F_0}{mM\omega^4 - 2k\omega^2(m+M)} \end{cases}.$$

Therefore, the displacements of the magnetic suspension stator and the stabilization mass block can be expressed as:

$$\begin{cases} x_1(t) = \dfrac{2kF_0}{mM\omega^4 - 2k\omega^2(m+M)} \sin \omega t \\ x_2(t) = \dfrac{(2k - m\omega^2)F_0}{mM\omega^4 - 2k\omega^2(m+M)} \sin \omega t \end{cases}.$$

According to the aforementioned formulas, the displacement simulation diagrams are obtained (Figures 3–5).

The velocities of the magnetic suspension stator and the stabilization mass block can be expressed as below, and their simulation diagrams are shown in Figure 4.

$$\begin{cases} \dot{x}_1(t) = \dfrac{2kF_0}{mM\omega^3 - 2k\omega(m+M)} \cos \omega t \\ \dot{x}_2(t) = \dfrac{(2k - m\omega^2)F_0}{mM\omega^3 - 2k\omega(m+M)} \cos \omega t \end{cases}.$$

The accelerations of the magnetic suspension stator and the stabilization mass block can be expressed as below, and their simulation diagrams are shown in Figure 5.

$$\begin{cases} \ddot{x}_1(t) = \dfrac{2kF_0}{2k(m+M) - mM\omega^2} \sin \omega t \\ \ddot{x}_2(t) = \dfrac{(2k - m\omega^2)F_0}{2k(m+M) - mM\omega^2} \sin \omega t \end{cases}.$$

(Simulation parameters are $k = 1 \times 10^5$N/m, $M = 1.26$ kg, $m = 0.225$ kg, $F = 10$ N in Figures 3–5.)

3.2 Mathematical model of the stabilizer and the ship

When the stabilizer is applied on the ship, its simplified mathematical model is shown in Figure 6, where m is the weight of stabilization mass block, M is the weight of ship, k_1 is the displacement stiffness coefficient between the stabilization mass block and hull, and k_2 is the displacement stiffness coefficient between hull and seawater. As the ship buoyancy force is $F = \rho g V = \rho g s x$, while $F = k_2 x$, the displacement stiffness coefficient of the ship in seawater is $k_2 = \rho g s$, about 1×10^4 sN/m, where ρ is the sea-water density, g is the acceleration of gravity, V is the volume of displacement, s is the cross-sectional area at the ship draft, damping influence is ignored, and the equations of motion are obtained as follows:

$$\begin{cases} m\ddot{x}_1(t) = k_1[x_2(t) - x_1(t)] \\ M\ddot{x}_2(t) = F_0 \sin \omega t - k_1[x_2(t) - x_1(t)] - k_2 x_2(t) \end{cases}. \quad (3)$$

Given

$$\begin{cases} x_1(t) = x_{10} \sin \omega t \\ x_2(t) = x_{20} \sin \omega t \end{cases}$$

is substituted into (3) and we get

$$\begin{cases} x_{10} = \dfrac{k_1 F_0}{Mm\omega^4 - (k_1 + k_2)m\omega^2 - k_1 M\omega^2 + k_1 k_2} \\ x_{20} = \dfrac{(k_1 - m\omega^2)F_0}{Mm\omega^4 - (k_1 + k_2)m\omega^2 - k_1 M\omega^2 + k_1 k_2} \end{cases}.$$

The displacements of the stabilizer and the ship can be expressed as below, and their simulation diagrams are shown in Figure 7.

$$\begin{cases} x_1(t) = x_{10} \sin \omega t = \dfrac{k_1 F_0 \sin \omega t}{Mm\omega^4 - (k_1 + k_2)m\omega^2 - k_1 M\omega^2 + k_1 k_2} \\ x_2(t) = x_{20} \sin \omega t = \dfrac{(k_1 - m\omega^2)F_0 \sin \omega t}{Mm\omega^4 - (k_1 + k_2)m\omega^2 - k_1 M\omega^2 + k_1 k_2} \end{cases}.$$

The velocities and accelerations of the stabilizer and the ship can be expressed as (4) and (5), and the acceleration simulation diagrams are shown in Figure 8.

$$\begin{cases} \dot{x}_1(t) = \omega x_{10} \cos \omega t \\ \qquad = \dfrac{\omega k_1 F_0 \cos \omega t}{Mm\omega^4 - (k_1 + k_2)m\omega^2 - k_1 M\omega^2 + k_1 k_2} \\ \dot{x}_2(t) = \omega x_{20} \cos \omega t \\ \qquad = \dfrac{\omega (k_1 - m\omega^2)F_0 \cos \omega t}{Mm\omega^4 - (k_1 + k_2)m\omega^2 - k_1 M\omega^2 + k_1 k_2} \end{cases} \quad (4)$$

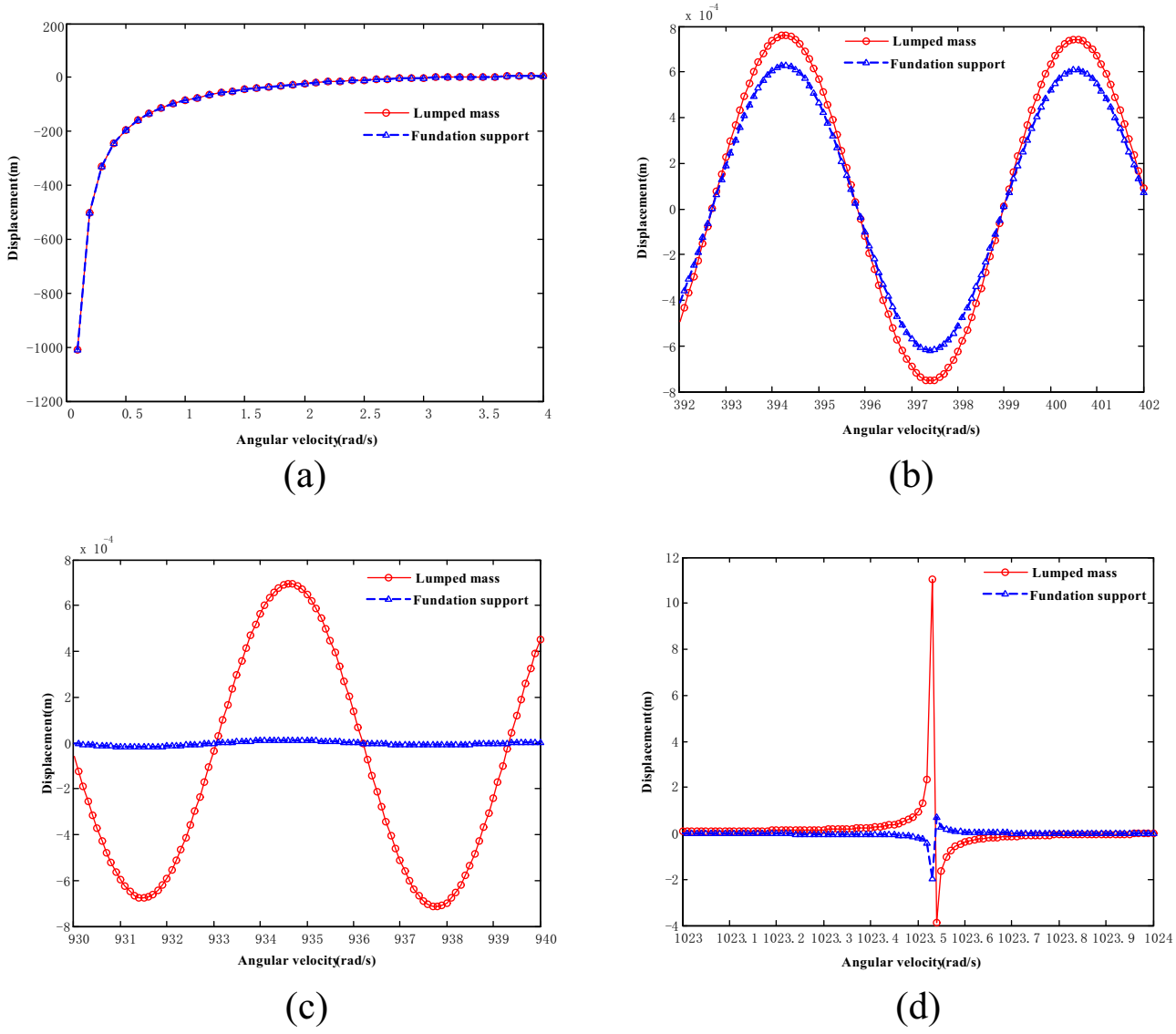

Figure 3: Displacement simulation diagram (a), (b), (c) and (d) of the magnetic suspension stator and the stabilization mass block at different angular velocities.

$$\begin{cases} \ddot{x}_2(t) = -\omega^2 x_{20} \sin \omega t \\ \quad = -\dfrac{\omega^2 k_1 F_0 \sin \omega t}{Mm\omega^4 - (k_1 + k_2)m\omega^2 - k_1 M\omega^2 + k_1 k_2} \\ \ddot{x}_1(t) = -\omega^2 x_{10} \sin \omega t \\ \quad = -\dfrac{\omega^2 (k_1 - m\omega^2) F_0 \sin \omega t}{Mm\omega^4 - (k_1 + k_2)m\omega^2 - k_1 M\omega^2 + k_1 k_2} \end{cases}. \quad (5)$$

(Simulation parameters are $k_1 = 8 \times 10^5$ N/m, $k_2 = 2 \times 10^5$ N/m, $M = 1{,}600$ kg, m = 400 kg, $F = 100$ N in Figures 7 and 8.)

3.3 Adaptive control based on frequency modulation

The displacement stiffness coefficient of the stabilization mass block is as follows:

$$k = -\frac{\mu_0 N^2 A i_{x_0}}{x_0^2}\frac{\mathrm{d}i}{\mathrm{d}x} + \frac{\mu_0 N^2 A i_{x_0}^2}{x_0^3}.$$

Considering the aforementioned formulas and the simulation of two systems, it can be known when the

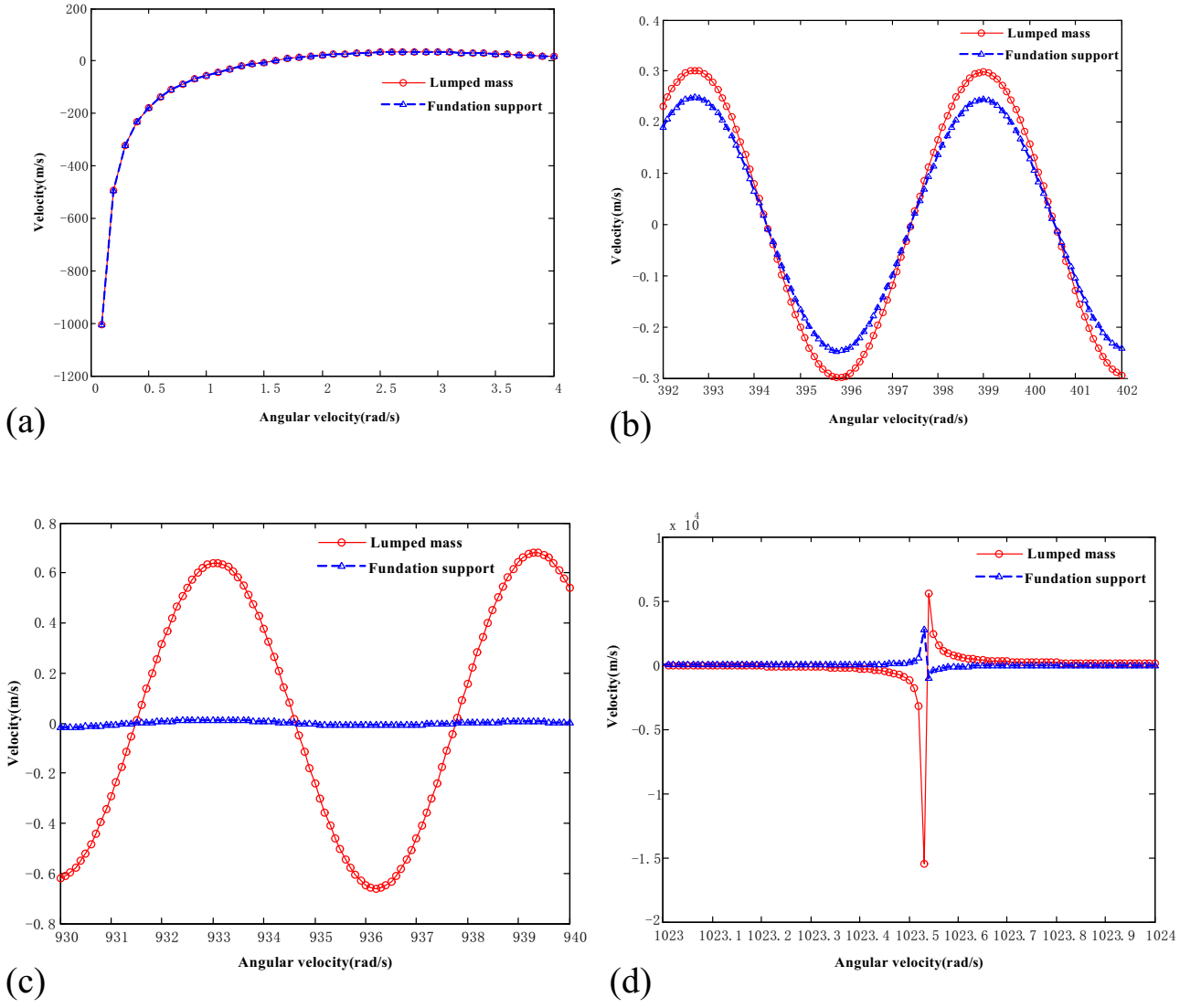

Figure 4: Velocity simulation diagram (a), (b), (c) and (d) of magnetic suspension stator and stabilization mass block at different angular velocities.

coil number of turns, pole area size, and the value of the bias current or air gap size of the stabilization mass block will be changed, the displacement stiffness coefficient of the stabilization mass block will be changed, and the natural frequency of the stabilization mass block will be changed too [15–19]. When a device is assembled, the coil number of turns and the size of the magnetic pole cannot be changed easily. In this study, the displacement stiffness coefficient is changed by changing the value of the bias current and the size of the air gap. By changing the thickness of the gasket between the shell and the cover, the air gap size of the device is adjustable. The thicknesses of gaskets are 2, 3, and 4 mm, respectively, in the experiment device.

Through the reference adaptive control, the adaptive controller is driven by the adaptive control error which is a different value between the object output and the reference value. By adjusting the parameters of the controller, the errors of the system are reduced, eventually the actual output of the controlled object is adjusted to the desired output. The diagram of the control system is shown in Figure 9, where I_r is the reference input of the system, y_p is the output of the controlled object, y_m is the output of the reference model, u is the control input of the controlled object, e is the system error, and e_m is the adaptive control error.

From Figures 3–5, 7, and 8, it can be known that three frequency bands deserve our attention. In Figures 3(c), 4(c), 5(c), 7(b), and 8(b), the vibration of the stabilization mass block (stabilizer) is more intense in this frequency band, but the base (hull) hardly vibrates.

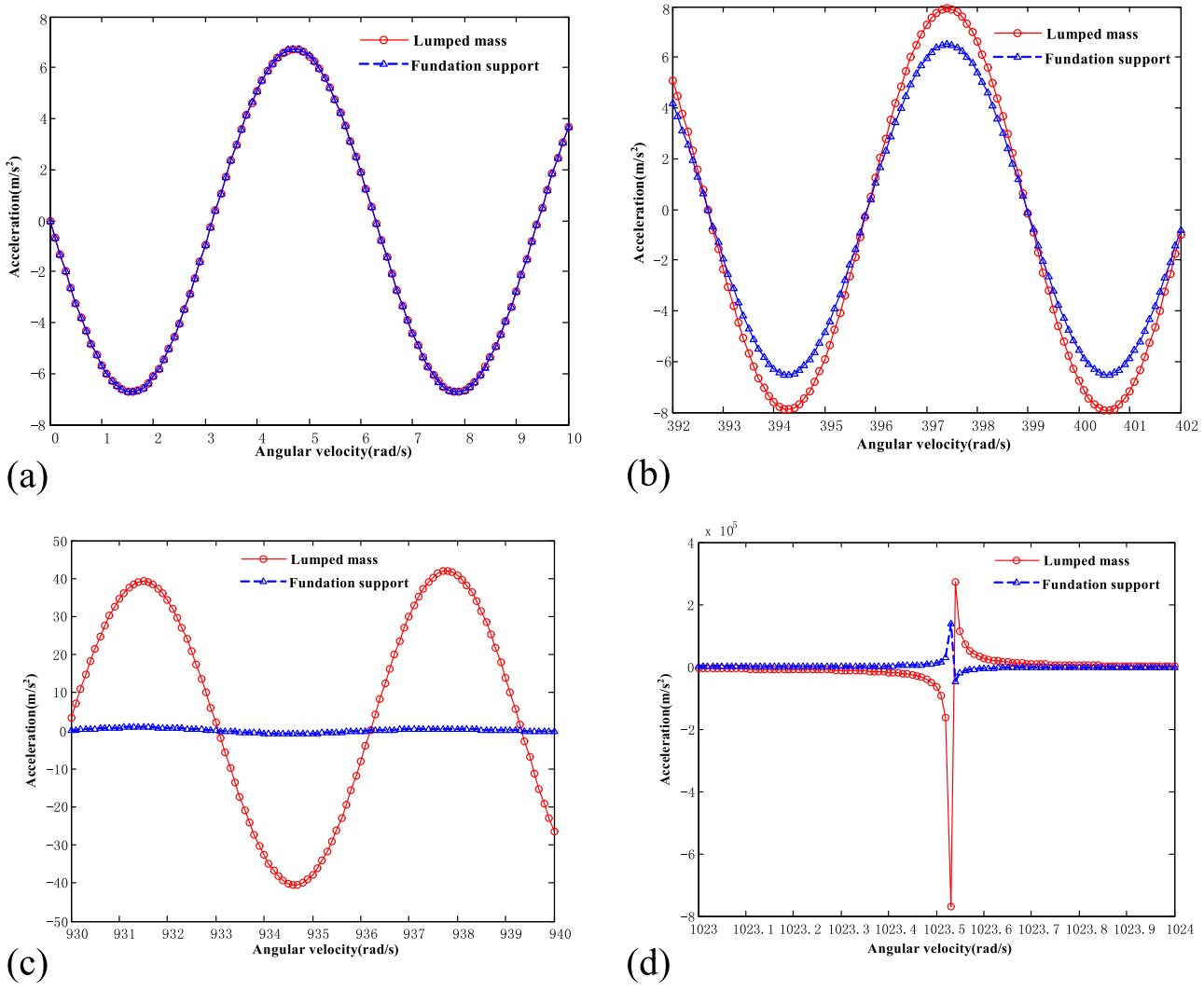

Figure 5: Acceleration simulation diagram (a), (b), (c) and (d) of magnetic suspension stator and stabilization mass block at different angular velocities.

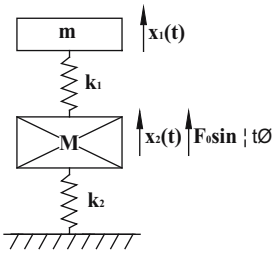

Figure 6: A simplified mathematical model of the stabilizer and the ship.

It is known that this frequency band is near the natural frequency of the stabilization mass block (stabilizer). That is, when the natural frequency of the stabilization mass block (stabilizer) is equal to or approximately the frequency of the disturbance, the external interference force that is the vibration energy is basically concentrated on the stabilization mass block.

In Figures 3(b), 4(b), 5(b), 7(a), and 8(a), the vibration of the stabilization mass block (stabilizer) and the base (hull) is more intense in this frequency band. It is obtained that the frequency band is near the natural frequency of the base (hull). When the natural frequency of the base (hull) is equal to or approximately the external disturbance frequency, the stabilization mass block (stabilizer) and the base (hull) synchronously vibrate.

It can be seen from Figures 3(d), 4(d), 5(d), 7(c), and 8(c) that the stabilization mass block (stabilize) and the base (hull) are vibrated very violently and that the frequency band is nearly equal to the natural frequency of the whole system. The system resonates when the natural frequency of the whole system is equal to or approximately the external disturbance frequency.

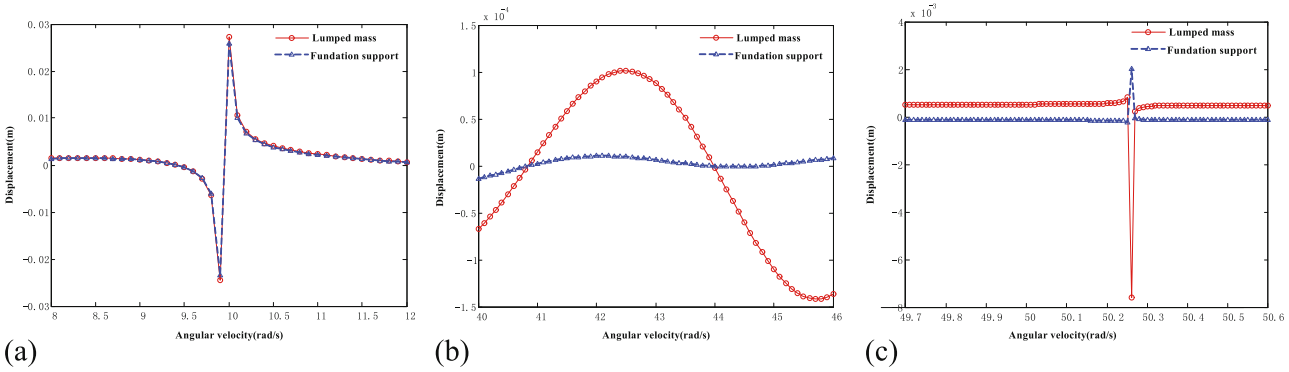

Figure 7: Displacement simulation diagram (a), (b) and (c) of stabilizer and ship at different angular velocities.

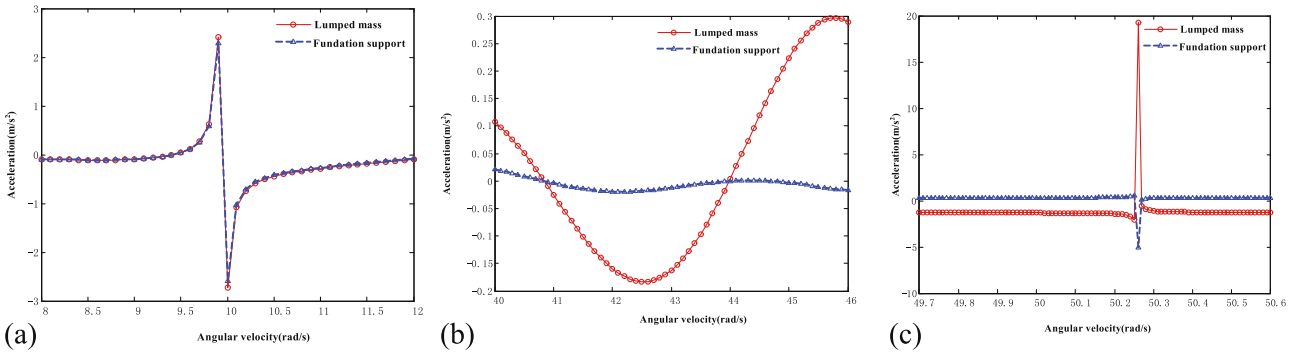

Figure 8: Acceleration simulation diagram (a), (b) and (c) of stabilizer and ship at different angular velocities.

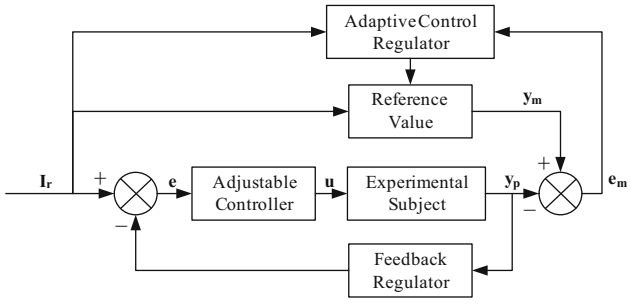

Figure 9: The diagram of the control system.

4 Experiments

On the basis of theoretical calculation, the authors have designed a set of magnetic suspension stabilizers and implemented component processing and assembling. The component diagram and assembly diagram are shown in Figure 10. Stable suspension experiment is first carried out when the device is assembled. On the basis of the stable suspension, acceleration values of the stator and the stabilization mass block are, respectively,

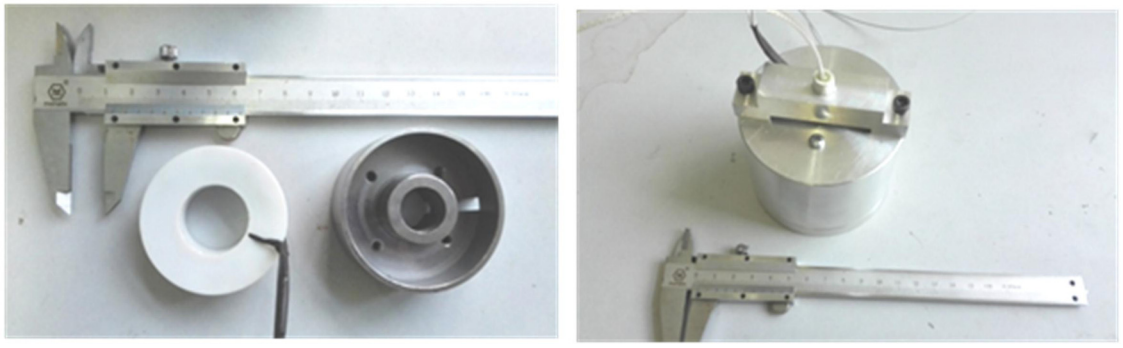

Figure 10: Parts and assembled parts of the magnetic suspension stabilizer.

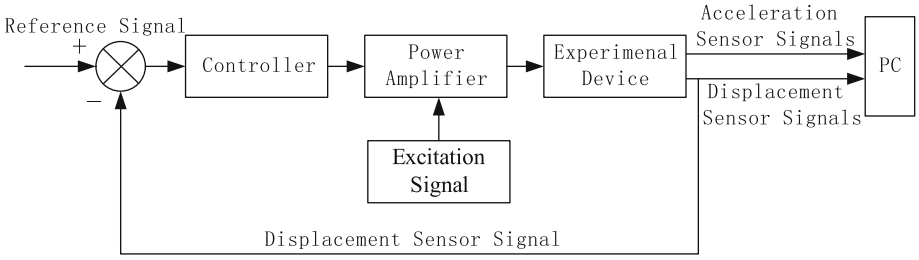

Figure 11: The block diagram of experiment.

Table 1: Parameter list of experiment

Parameter	Value
N	138
Wire diameter	1 mm^2
Upper bias current	1.5 A
Lower bias current	1.5 A
Stator	1259 g
Rump mass	225 g
Gap	0.5 mm
Excitation amplitude	500 mV
Excitation frequency	0–500 Hz
Accelerometer	ADXL335B

measured by loading 0–500 Hz sine voltage excitation signal on electromagnetic coil. The block diagram of the experiment is shown in Figure 11, and its specific parameters are shown in Table 1; field test and acceleration oscillograms are shown in Figures 12–15.

It can be seen from Figure 13 that the stabilization mass block and the base hardly vibrate. Figure 14 shows that the stabilization mass block vibrated very violently, and its acceleration value is approximately 0.94 g. Figure 15 shows that both the stabilization mass block and the base vibrated hardly, and their acceleration values are approximately 0.48 and 0.33 g.

5 Conclusions

(1) According to the simulation and test data, when the natural frequency of the stabilization mass block is equal to or approximately the disturbance frequency of the outside, the base (hull) almost do not vibrate, and the external interference force that is the vibration energy is basically concentrated on the stabilization mass block.
(2) When the disturbing force frequency changed, through the adaptive control algorithm, the natural frequency of the stabilization mass block can be adjusted to be similar to the outside disturbance frequency. Then the system will have a very good stabilizing effect.
(3) When the magnetic suspension stabilization technology is applied on the ship, as long as the natural frequency of the stabilization mass block is equal to the wave frequency, it will have a good stabilizing effect regardless of the ship at the zero speed, low speed, and high speed.

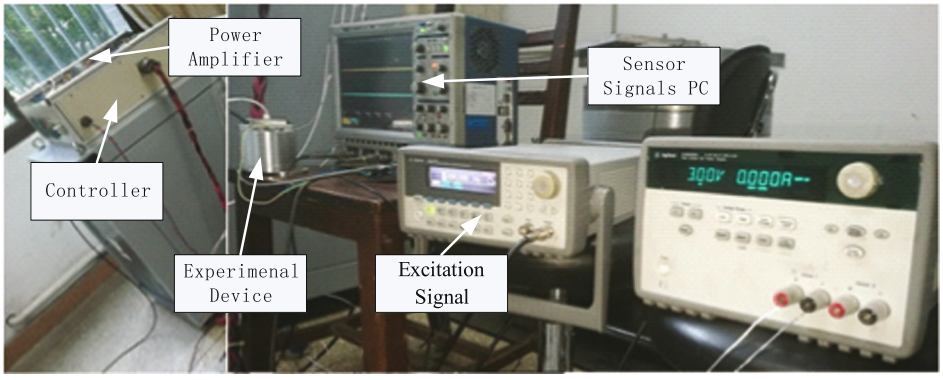

Figure 12: Field test.

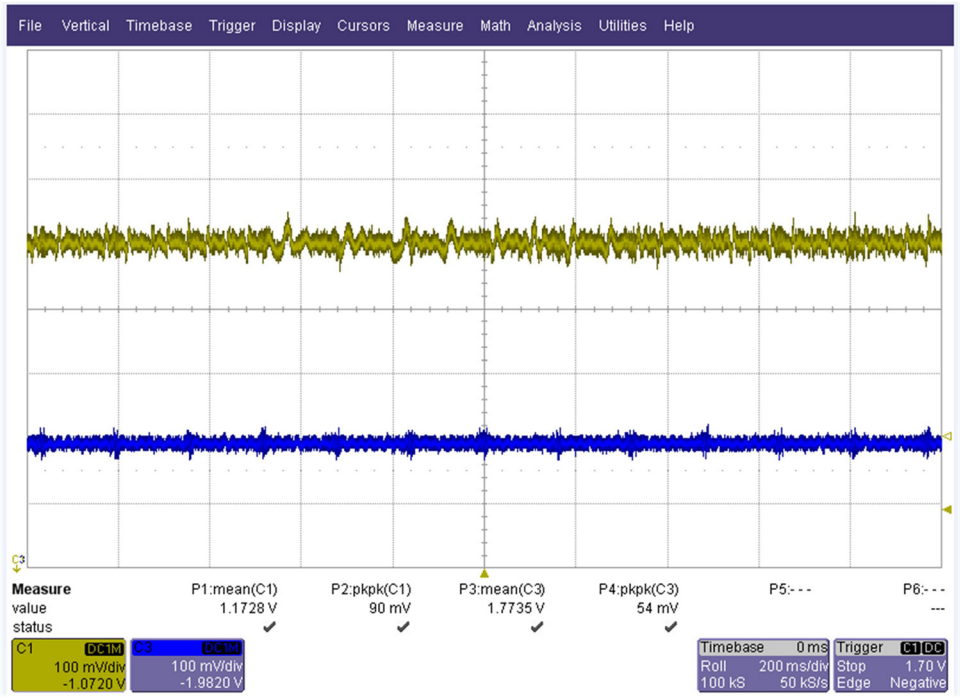

Figure 13: Acceleration diagram of the stabilization mass block and base at the excitation voltage of 1 Hz.

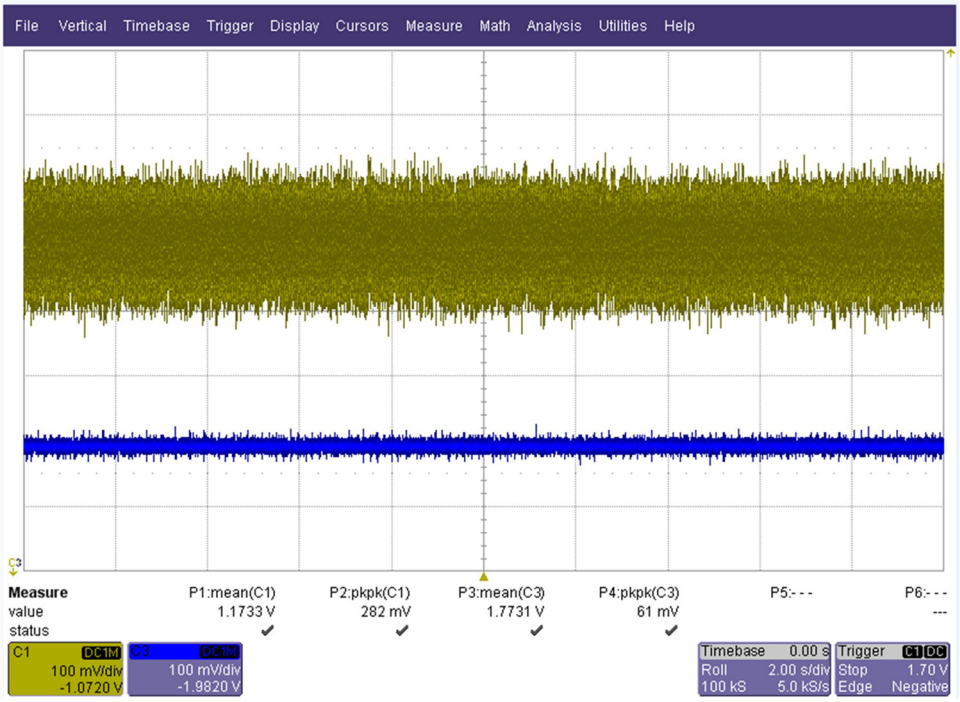

Figure 14: Acceleration diagram of the stabilization mass block and base at the excitation voltage of 57 Hz.

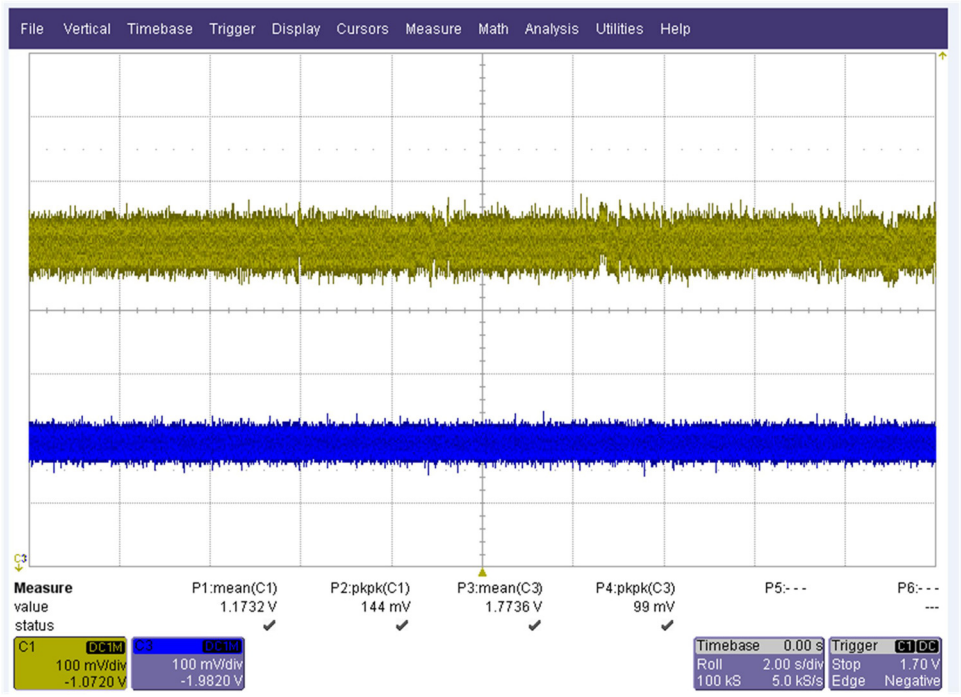

Figure 15: Acceleration diagram of the stabilization mass block and base at the excitation voltage of 156 Hz.

Acknowledgement: This project was supported by the National Natural Science Foundation of China (Grant No. 51675261) and the Natural Science Foundation of Jiangsu Province (BK20161102).

References

[1] Perez T. Ship Motion Control. London: Springer-Verlag; 2005.
[2] Yu YH. Prediction of flows around ship-shaped hull sections in roll using anunsteady Navier-Stokes solver. Doctor dissertation, The University of Texas at Austin; 2008.
[3] Luo WL, Hu BB, Li TS. Neural network based fin control for ship roll stabilization with guaranteed robustness. Neurocomputing. 2017;230:210–8.
[4] Taskar BU, Dasgupta D, Nagarajan V, Suman C, Anindya C, Om PS. CFD aided modeling of anti-rolling tanks towards more accurate ship dynamics. Ocean Eng. 2014;92:296–303.
[5] Cercos-Pita JL, Bulian G, Pérez-Rojas L, Francescutto A. Coupled simulation of nonlinear ship motions and a free surface tank. Ocean Eng. 2016;120:281–8.
[6] Neves Marcelo AS, Merino Jorge A, Rodríguez Claudio A. A nonlinear model of parametric rolling stabilization by anti-roll tanks. Ocean Eng. 2009;36:1048–59.
[7] Kallstrom CG. Control of yaw and roll by rudder/fin stabilization system. Proc SCSS'81, Can. 1981;12:3–14.
[8] Terao Y. The system simulation and sea test of a new type of passive controllable stabilization tank. Kansai Shipbuild Assoc J. 1993;219:75–88.
[9] Senjanomc I, Parunov J, Cipric G. Safety analysis of ship rolling in rough sea. Chaos Solitons & Fractals, UK. 1997;8(4):659–80.
[10] Chen F, Lai ZC. The application of parameter frequency response method in "double-tank" system. J Ship Mech. 2003;1:38–45.
[11] Zhao WP. Research on integrated balance system of large surface warship. Doctoral Dissertation. Harbin Engineering University; 2004.
[12] Park CH, Park HC, Cho HW, Moos SJ, Chunq TY. Development of a small maglev-type antirolling system. Rev Sci Instrum. 2010;81:056102.
[13] Hirakawa Y, Hirayama T, Kakizoe K, Takayama T, Funamizu S, Okada N, et al. Sea trial of prototype vertical weight stabilizer (VWS) anti-rolling system for small ships. J Mar Sci Technol. 2014;19:292–301.
[14] Hu YF, Zhou ZD, Jiang ZF. Basic theory and application of magnetic bearing. Beijing, China: China Machine Press; 2006.
[15] Akyildiz FT, Vajravelu K. Galerkin-chebyshev pseudo spectral method and a split step new approach for a class of two dimensional semi-linear parabolic equations of second order. Appl Mathematics & Nonlinear Sci. 2018;3:255–64.
[16] Cao L, Tu C, Hu P, Liu S. Influence of solid particle erosion (SPE) on safety and economy of steam turbines. Appl Therm Eng. 2019;150:552–63.
[17] Devaki P, Sreenadh S, Vajravelu K, Prasad KV and Vaidya H. Wall properties and slip consequences on peristaltic transport of a casson liquid in a flexible channel with heat transfer. Appl Mathematics & Nonlinear Sci. 2018;3:277–90.
[18] Lokesha V, Shruti R, Deepika T. Reckoning of the dissimilar topological indices of human liver. Appl Mathematics & Nonlinear Sci. 2018;3:265–76.
[19] Vajravelu K, Li R, Dewasurendra M, Benarroch J, Ossi N, Zhang Y, et al. effects of second-order slip and drag reduction in boundary layer flows. Appl Mathematics & Nonlinear Sci. 2018;3:291–302.